National Scale Surface Deformation Time Series Generation through Advanced DInSAR Processing of Sentinel-1 Data within a Cloud Computing Environment

I. Zinno, M. Bonano, S. Buonanno, F. Casu, C. De Luca, M. Manunta, M. Manzo, and R. Lanari, *Fellow, IEEE*

Abstract—We present an automatic pipeline implemented within the Amazon Web Services (AWS) Cloud Computing platform for the interferometric processing of large Sentinel-1 (S1) multi-temporal SAR datasets, aimed at analyzing Earth surface deformation phenomena at wide spatial scale. The developed processing chain is based on the advanced DInSAR approach referred to as Small BAseline Subset (SBAS) technique, which allows producing, with centimeter to millimeter accuracy, surface deformation time series and the corresponding mean velocity maps from a temporal sequence of SAR images. The implemented solution addresses the aspects relevant to i) S1 input data archiving; ii) interferometric processing of S1 data sequences, performed in parallel on the AWS computing nodes through both multi-node and multi-core programming techniques; iii) storage of the generated interferometric products. The experimental results are focused on a national scale DInSAR analysis performed over the whole Italian territory by processing 18 S1 slices acquired from descending orbits between March 2015 and April 2017, corresponding to 2612 S1 acquisitions. Our analysis clearly shows that an effective integration of advanced remote sensing methods and new ICT technologies can successfully contribute to deeply investigate the Earth System processes and to address new challenges within the Big Data EO scenario.

Index Terms—Big data, Cloud Computing, DInSAR, P-SBAS, Earth surface deformation, Synthetic Aperture Radar, time series

1 Introduction

The Big Data paradigm is bringing revolutions in many scientific fields [1], [2], [3], [4], [5], [6]. A very relevant one is represented by Earth Observation (EO) where it is opening promising investigation opportunities and facing new challenges [7], [8]. Among several applications, the EO techniques have already shown to be very powerful for the detection and analysis of surface deformations due to their characteristics of large spatial coverage, high accuracy and cost effectiveness. The investigation of Earth's surface deformation phenomena provides critical insights into several processes of great interest for science and society, especially from the perspective of further understanding the Earth System [9], [10], [11], [12], [13], [14], [15], [16], [17] and the impact of human activities [18], [19], [20], [21], [22], [23], [24], [25]. In this scenario, Differential Synthetic Aperture Radar Interferometry (DInSAR) is regarded as one of the key EO methods for its ability to investigate surface displacements affecting large areas of the Earth with centimeter- to millimeter-level accuracy [26], [27], [28].

Basically, the DInSAR technique allows generating spatially dense deformation maps by exploiting the phase difference (interferogram) between pairs of complex SAR images, usually referred to as Single Look Complex (SLC) images. They are relevant to acquisitions carried out at different times but with nearly the same illumination geometry and from sufficiently close flight tracks, whose separation is typically referred to as baseline [27], [28], [29], [30]. More specifically, the DInSAR methodology analyzes the "differential" interferograms generated through the difference between an interferogram and its topography-related phase component [31], the latter being calculated by exploiting the sensor orbital information and an external Digital Elevation Model (DEM) of the illuminated area. Note that, for the sake of simplicity, in the following of this paper the terms interferogram and differential interferogram will be considered as synonyms. Note also that the DInSAR technique permits to estimate the surface displacements component along the radar line of sight (LOS) and it effectively works in areas where the computed interferograms are characterized by high coherence, i.e., in zones that are not significantly affected by phase noise effects, usually referred to as decorrelation phenomena [32].

- *I. Zinno, S. Buonanno, F. Casu, C. De Luca, M. Manunta, M. Manzo and R. Lanari are with the IREA, CNR, Napoli, Italy. E-mail: {zinno.i, bonano.m, casu.f, deluca.c, manunta.m, manzo.m, lanari.r}@irea.cnr.it.*
- *M. Bonano is with the IREA, CNR, Napoli, Italy, and also with the IMAA, CNR, Tito Scalo, Italy. E-mail: manuela.bonano@imaa.cnr.it.*

Manuscript received 1 Mar. 2018; revised 19 June 2018; accepted 17 July 2018. Date of publication 17 Sept. 2018; date of current version 29 Aug. 2020. (Corresponding author: Ivana Zinno.)
Recommended for acceptance by M. Datcu, J. Le Moigne, P. Soille, P. G. Marchetti, and G.-S. Xia.
Digital Object Identifier no. 10.1109/TBDATA.2018.2863558

The DInSAR methodology has been originally applied to analyze single deformation episodes such as earthquakes and volcanic unrests [9], [10], [12], [33]. However, thanks to the availability of long SAR data time series, it is also possible to study the temporal evolution of the detected surface deformations. This is carried out through the exploitation of the so-called advanced DInSAR techniques, which properly combine the information available from a set of multi-temporal interferograms relevant to an area of interest, in order to compute the deformation time series [34], [35], [36], [37], [38], [39], [40], [41]. Among several advanced DInSAR algorithms, a widely used approach is the Small BAseline Subset (SBAS) technique [37], which generates LOS-projected deformation time series and the corresponding mean deformation velocity maps by exploiting interferograms characterized by small temporal and/or spatial baselines between the acquisition orbits, in order to mitigate the decorrelation phenomena. The SBAS algorithm has already proven its effectiveness to investigate surface displacements with millimeters accuracy [42], [43] in different scenarios, such as volcanoes, tectonics, landslides, anthropogenic induced land motions [44], [45], [46], [47], [48], [49], [50], [51], [52], [53], and it is capable to perform analyses at different spatial scales [38], [54] and with multi-sensor data [55], [56].

Currently, the DInSAR scenario is characterized by a huge availability of SAR data acquired during the last 25 years, comprising the long-term C-band European Space Agency (ESA) archives (e.g., ERS-1, ERS-2, and ENVISAT), the RADARSAT-1 and RADARSAT-2 C-band data sequences, those provided by the L-band ALOS-1 and ALOS-2 sensors and by the X-band generation of SAR sensors, such as the COSMO-SkyMed (CSK) and TerraSAR-X constellations. Moreover, a massive and ever increasing data flow is nowadays supplied by the C-band Sentinel-1 (S1) constellation of the European Copernicus program that is composed of two twin SAR satellites, Sentinel-1A and Sentinel-1B, which have been launched on April 2014 and April 2016, respectively [57]. The main S1 acquisition mode on land, referred to as Interferometric Wide Swath (IWS), implements the Terrain Observation by Progressive Scans (TOPS) technique [58]; this is specifically designed for interferometric applications and guarantees a very large spatial coverage: indeed, the nominal footprint of the S1 TOPS mode extends for about 250 km, thus allowing the constellation to operate with a global coverage acquisition strategy. The S1 interferometric revisit time is either 12 or 6 days in the case of one or two operating satellites, respectively. Moreover, the S1 constellation is also characterized by a very short orbital tube, with a diameter of about 200 m. Therefore, thanks to both its small spatial and temporal baselines, the S1 constellation is specifically oriented to DInSAR applications and, in particular, it naturally fits the SBAS approach characteristics. In addition, it is worth noting that the whole S1 archive is available with a free and open access policy, thus easing the data access and enlarging the scientific community interested in its exploitation, opening new research perspectives to understand Earth's surface deformation dynamics at global scale. It is also evident that the S1 EO constellation, providing nowadays about 10 TB per day, is significantly contributing to move Earth Observation toward the Big Data "V" concept. Indeed, managing and storing the involved, huge amount of data (Volume), processing it in an efficient way (Velocity) and maximizing the available archives exploitation (Variety) are becoming high priority issues (Big Data "V") [59].

By considering the above described DInSAR scenario, it is clear that the development of effective solutions able to properly deal with the transfer, the storage, and, above all, the processing of such a huge SAR data flow is strongly needed. Within the framework of the advanced DInSAR processing, a parallel algorithmic solution for the SBAS approach, referred to as Parallel Small BAseline Subset (P-SBAS), which implements a complete advanced DInSAR processing chain (starting from either RAW or SLC data and ending with deformation time series generation) and is able to exploit distributed computing architectures, has been recently developed [60]. P-SBAS permits to generate, in an automatic and unsupervised way, advanced DInSAR products by taking full benefit from parallel computing architectures, such as cluster and grid infrastructures. This solution has also been implemented within the ESA Grid Processing on Demand (G-POD) environment [61] and the Geohazard Exploitation Platform (GEP) [62] to make available the SBAS technique for on-demand processing [63].

However, within the Big Data context, the exploitation of Cloud Computing (CC) infrastructures definitely represents an effective solution to properly deal with all the issues related to very large volumes of EO data [6]. Indeed, CC provides highly scalable and flexible architectures that are, in general, computationally very efficient and, in several cases, less expensive with respect to in-house solutions. Moreover, the increasing availability of CC environments, and their relative simplicity to use, is further pushing toward the use of such a technology also in scientific applications [64]. In this scenario, we already developed some works regarding the migration of the P-SBAS processing chain to the Amazon Web Services (AWS) CC environment [65], [66]. These works concerned the evaluation of the P-SBAS parallel performances achievable within a CC infrastructure and the subsequent identification of the main issues affecting the P-SBAS scalability, i.e., the capability to efficiently use increasing resources in order to sustain the processing of Big Data volumes and to reduce the computing elapsed times [67], [68], [69].

Leveraging the above-mentioned considerations relevant to the migration to CC environments, we present in this work the implementation of an interferometric processing chain based on the P-SBAS approach dedicated to the processing of S1 data within the AWS environment. It supports both multi-node and multi-core scheduling policies and permits to generate surface deformation time series from large volumes of S1 data, thus allowing us to perform national-scale DInSAR analyses. It is worth noting that the proposed S1 data interferometric processing chain deals with all the aspects relevant to the i) S1 input data archiving, ii) their processing and iii) the storage of the computed interferometric products. In particular, we developed an automatic pipeline, which includes the download of the S1 input data from the AWS S3 [66] archive towards the computing nodes, the launch and the completion of the P-SBAS DInSAR processing and, finally, the transfer of the generated results to the S3 long-term storage.

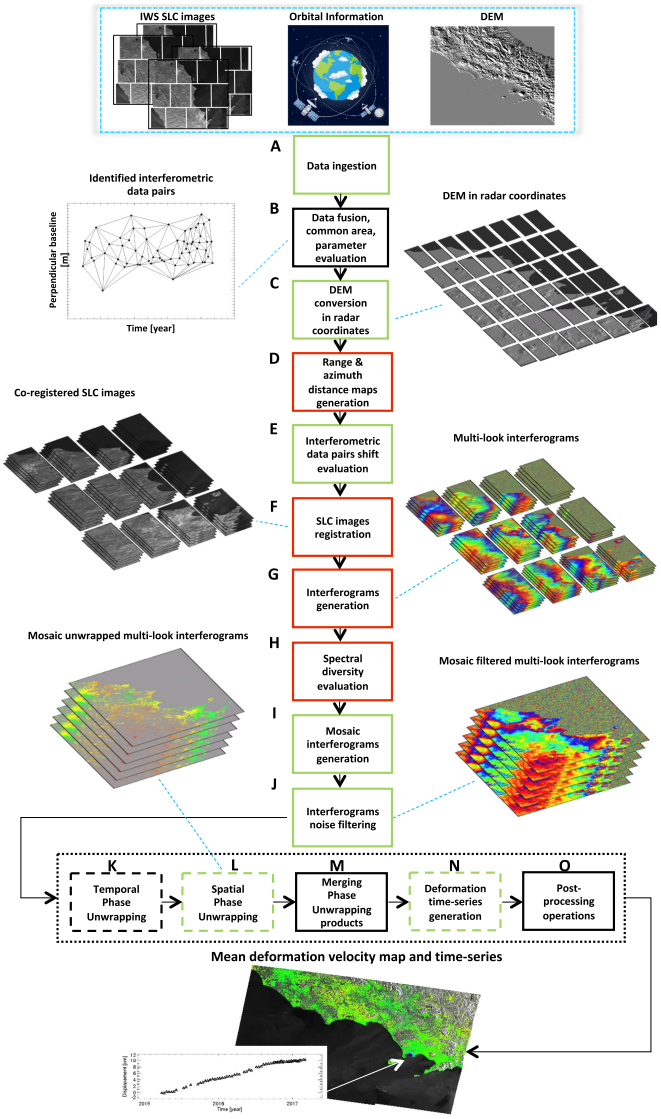

Fig. 1. Block diagram of the S1 P-SBAS processing chain. Green and red blocks represent the processing steps that are executed in parallel by splitting the computation on subsets of input data (subsets of bursts, subsets of SLC images, interferograms or other interferometric products). Dashed line blocks represent processing steps benefiting also from multi-threading programming. Black blocks stand for the processing steps that are sequentially executed.

As experimental results we show in this paper the national scale DInSAR analysis performed over the Italian territory by processing 18 S1 slices (where a slice indicates an area on the ground of about 250 $\times$ 250 km^2) acquired from descending orbits during the March 2015-April 2017 time span, corresponding on the whole to 2612 S1 IWS SLC images. Such an analysis was entirely carried out by exploiting AWS storage and computing resources.

The manuscript is organized as follows. In Section 2 we describe the interferometric processing chain developed to process large S1 SAR dataset based on the P-SBAS approach [60]. In Section 3, the implementation of the S1 P-SBAS processing chain within the AWS CC environment is discussed. Section 4 is dedicated to present the achieved experimental results and, finally, in Section 5 we draw some conclusions on the further developments of the presented work.

2 The S1 P-SBAS Processing Chain

This section is aimed at concisely describing the interferometric processing chain based on the P-SBAS approach [60] developed to process large S1 SAR datasets. The P-SBAS algorithm was originally designed to efficiently exploit distributed computing infrastructures for the automatic processing of SAR images acquired through the Stripmap mode, and it has been largely tested with ENVISAT and COSMO-SkyMed SAR datasets [63], [67], [68], [69], [70]. Here, we present the main modifications applied to the P-SBAS Stripmap processing chain in order to handle S1 IWS SAR data, which are collected through the TOPS acquisition mode [58] and, therefore, are composed by several bursts, which can be treated as independent portions of data.

The presented S1 P-SBAS interferometric processing chain strongly benefits from this particular structure of the S1 IWS data that makes the computation intrinsically parallelizable with respect to the independent bursts. Accordingly, the coarse-grained parallelization strategy adopted in [60] for the Stripmap data can be extended at the burst level in a large number of the S1 P-SBAS processing steps. It is worth noting that, as discussed in the following, similarly to the original P-SBAS chain, a finer granularity parallelization strategy is also considered for the steps that are particularly intensive from the computational viewpoint, by exploiting both multi-node and multi-core programming techniques.

Let us start our analysis from the block diagram of the implemented S1 P-SBAS processing chain, which is shown in Fig. 1. This scheme basically follows the original P-SBAS one [60], [68], from which it mainly differs for the lack of the raw data focusing step, since in the S1 case we directly exploit SLC products, as well as for the image registration and interferogram generation steps, which are significantly modified with respect to the original Stripmap-like P-SBAS chain to take into account the specific peculiarities of the TOPS acquisition mode.

Within this scheme, the blocks of the P-SBAS processing chain depicted by red color represent the jobs parallelized at burst level (the coarse-grained parallelization mentioned above); moreover, the green color blocks stand for the jobs that are parallelized with respect to portions of other kinds of input data, which can be either SLC images, interferograms, or other intermediate products, depending on the specific processing step. Both green and red blocks can be executed in parallel by splitting the concurrent jobs on either multiple nodes or different CPUs. The black blocks, instead, represent steps that are intrinsically sequential, as they typically merge together and perform operations on data and intermediate products deriving from previous steps. Moreover, in Fig. 1, the blocks outlined with the dashed line symbolize steps in which also finer-grained parallelization strategies are implemented by exploiting multithreading programming techniques and tools able to efficiently manage the most intensive computing operations.

The S1 P-SBAS processing chain workflow starts first with handling and ingesting the input data, which are represented by (see the blue dashed box in Fig. 1): i) a sequence of S1 IWS SLC images, collected from the same acquisition orbits over an area of interest, ii) the orbital information associated to each SAR acquisition, and iii) the Digital

Elevation Model (DEM) of the investigated area, which usually comes out from the mosaicking of different DEM patches covering the zone of interest.

Concerning the description of the processing steps, in the following we briefly illustrate the operations performed by each of them, by also highlighting the kind of implemented parallelization strategy.

Step A carries out the S1 data ingestion and unpacking, corresponding to the extraction of each SLC image—in particular, of the relevant bursts—from the original (standard format) files. It is executed in parallel on subsets of the input SLC image dataset.

Step B deals with the extraction of the orbital information for each S1 SLC input data; moreover, it implements the identification of the reference (master) SAR geometry (i.e., the SAR acquisition chosen as reference geometry for the registration step), as well as of the interferometric SAR data pairs. Note that, thanks to the characteristics of the S1 constellation (very small orbital tube and down to 6 days revisit time over wide areas, including Europe), it is possible to constrain the analysis on small baseline interferograms [37], thus minimizing the spatial decorrelation effects [32]. At the same time, Step B identifies the area of interest common to the whole available SAR dataset, thus identifying the actual bursts to be processed. Finally, if the investigated area involves more than one S1 slice, the fusion of the SLC data relevant to consecutive slices is performed. Step B is sequentially executed.

Step C performs the DEM conversion into the radar (azimuth and range) coordinates by exploiting the range-Doppler equations [71]. This step is executed in parallel, indeed the initial DEM matrix is divided into small patches on which the computation is concurrently performed.

Step D computes the matrices containing, for each pixel of the SAR images, the information relevant to the distance between the target and the SAR sensor position (range distance) in the plane perpendicular to the sensor flight path (i.e., zero Doppler plane), as well as the azimuth distance between each pixel and a selected reference position along the acquisition orbit [72]; these matrices are usually referred to as range and azimuth files. Step D is executed in parallel at burst level.

Step E deals with the evaluation of the sub-pixel shifts needed to achieve the registration of the SLC images with respect to the master one. It is implemented by exploiting the orbital information and by maximizing the interferometric coherence for a reference burst of each interferometric pair identified in the previous Step B. This step is parallelized at interferogram level.

Step F performs the interpolation requested to obtain the registration [72] of the exploited SAR images with respect to the reference SAR geometry. To this aim, it exploits the previously computed azimuth/range information, the sub-pixel shifts and the S1 SLC sequence, and provides a set of registered SLC images. This step is executed in parallel at burst level.

Step G computes the differential interferograms (whose list has been identified from the interferometric data pairs selection carried out in Step B) starting from the registered SLC images and the corresponding range information. In this case we compute the phase difference between the selected full resolution S1 interferometric image pairs. Subsequently, a spatial average (multi-look) operation [31] is performed on the full resolution interferograms before storing the achieved results; this step is aimed at mitigating the decorrelation noise affecting the computed interferograms and to drastically reduce the amount of data to be later processed. This step is executed in parallel at burst level.

Step H deals with the retrieval (via the Spectral Diversity method [73]) and the subsequent removal of residual phase ramps from the interferometric phase signals due to possible residual mis-registration errors. This step is executed in parallel at burst level.

Step I implements the mosaicking of the achieved interferometric burst products (multi-looked interferograms and spatial coherence maps for each burst) in order to generate the overall DInSAR maps covering the whole investigated area. This step is executed in parallel at interferogram level.

Step J performs a further noise reduction operation on the retrieved DInSAR interferograms by applying the filtering technique proposed in [74], [75]. Step J is executed in parallel at interferogram level.

Steps K-O deal with the generation of the deformation time series and the corresponding mean deformation velocity maps starting from the computed sequence of differential interferograms, by involving both multi-node and multithreading parallelization strategies. More in details, Steps K and L perform the Phase Unwrapping (PhU) operations by applying the Extended Minimum Cost Flow (EMCF) algorithm [76], in order to retrieve the original (unwrapped) phase from the modulo-2π (wrapped) one. In particular, the exploited algorithm consists of the solution of two separate networks defined in the temporal/perpendicular baseline and in the azimuth/range domains [76]. More specifically, Step K performs the temporal PhU by simultaneously exploiting, for each coherent SAR pixel, all the wrapped DInSAR interferograms and generates a set of three-dimensional (3-D) matrices containing the information needed for the subsequent step of the processing chain. Step K exploits a multithreading parallelization strategy.

Step L operates on the 3-D matrices computed by Step K and performs the spatial PhU operation [77]. It benefits from a dual level of parallelization, a coarser one based on distributing in parallel the computation of these 3-D matrices, and a finer one that allows processing portions of these matrices through multithreading techniques.

Step M merges the results of the previously performed PhU procedure to achieve the final unwrapped differential interferogram sequence; the latter is, in turn, portioned in 3-D matrices in order to carry out in parallel the subsequent operations. Step M is sequentially executed.

Step N first inverts each of the so-identified 3-D matrices (each one containing a portion of the sequence of unwrapped interferograms) by applying the Singular Value Decomposition (SVD) method, and then joins the achieved results, thus leading to the generation of the final outputs, i.e., the deformation time series [37]. Moreover, Step N computes the temporal coherence factor [76], which gives information about the constancy of the computed displacement measurements with respect to the sequence of generated interferograms. This step is characterized by a dual-level parallelization realized as described for Step L.

Step O consists of a post-processing operation aimed at improving the quality of the retrieved deformation timeseries. In particular, it deals with the detection and removal of possible undesired atmospheric artifacts following the lines of [37]. This step is sequentially executed and provides the final (atmospheric disturbance filtered) deformation time series and mean displacement velocity maps.

3 The S1 P-SBAS Cloud Implementation within Amazon Web Services

This section is aimed at describing the CC based implementation of the S1 P-SBAS processing chain presented in the block diagram of Fig. 1 and described in details in Section 2. As a CC provider we choose the AWS Elastic Cloud Compute (EC2) environment [78] that is one of the most relevant players in the market. The main issues related to the migration to a CC platform of an interferometric processing chain like the P-SBAS one, dealing with large dataset of SAR images, are the following [7]:

- the input data storage and their transfer to the computing nodes. This operation, due to the involved large volumes (from hundreds of GB to several TB), can take a time comparable and even larger than the computational one, if the network is not highly performing;
- the management of the parallel tasks of the computation. Indeed, depending on the parallelization strategies adopted throughout the P-SBAS processing chain, which are different among the several steps, the scheduling of the jobs running on the CC platform has to be properly designed. In particular, aspects such as RAM use, CPUs exploitation and Input/Output (I/O) bandwidth occupation should be carefully taken into account when deciding whether to use either multiple nodes or multiple cores for the computation;
- the storage of the results and products generated by the processing.

Regarding the first issue, it is very important to have the S1 input data stored "in proximity" of the computing facilities to be used for the processing. This means to have both the data as close as possible to the computing nodes and the capacity to transfer them with a high velocity. Therefore, we created an archive of S1 data on the Simple Storage Service (S3) of AWS [66], which is a long-term, inexpensive storage having a theoretically infinite network bandwidth in connection to the EC2 Cloud resources. We located our archive in the Ireland EU-West region, which is where we reserved the computing nodes as well. At present, the archive contains all the S1 IWS SLC images acquired over Italy and it is updated with new acquisitions every time new data on the S1 catalogue [79] are available.

Concerning the scheduling and the distribution of the parallel tasks of the P-SBAS processing chain, we have to take into account that, as explained in Section 2, the parallelization strategy dominating the P-SBAS processing chain is the coarse-grained one, based on splitting the input datasets of each processing step in chunks of data to be processed in parallel. Indeed, although some steps may benefit from a further level of parallelization with a finer granularity, by exploiting specific multithreading programming techniques, the totality of the P-SBAS parallel steps can be made parallel by distributing the processing of portions of the input data among different processors. In particular, as discussed in the previous section, several steps (blocks D, F, G and H in Fig. 1) take advantage of the intrinsic partition of S1 IWS images in bursts as independent portions of data to be processed in parallel, whereas in other steps we split the processing operations relevant to portions of SLC images, interferograms or more complex structures of data (blocks A, C, E, I, J, L and N of Fig. 1, respectively).

TABLE 1
Average Requirements of the P-SBAS Algorithm for Each Step of the Block Diagram Shown in Fig. 1

Step	seq/par /multi-th	% CPU	RAM (MB)	File System Input*	File System Output*
A	par	130	1,300/1,500	50×10^6	100×10^6
B	seq	400/500	25,000/30,000	$1{,}500 \times 10^6$	$2{,}000 \times 10^6$
C	par	100	600	0	3×10^6
D	par	150/200	5,000	< 100	1.5×10^6
E	par	120	25,000/30,000	$< 500{,}000$	2×10^6
F	par	100	15,000/20,000	1.5×10^6	3×10^6
G	par	200/250	1,000/1,500	15×10^6	6×10^6
H	par	100	1,00/1,500	2×10^6	150,000
I	par	120	600	140.81	300,000
J	par	120	10,000/15,000	6×10^6	15×10^6
K	multi-th	2800/3000	30,000	200,000	200×10^6
L	par/multi-th	600/800	80,000	300×10^6	20×10^6
M	seq	1200/1500	15,000/20,000	250×10^6	20×10^6
N	par/multi-th	100	50	0	6,000
O	seq	800	20,000	10,000	60×10^6

Note that the file system inputs and the file system outputs are evaluated as non cached reads in 512-byte blocks and non cached writes in 512-byte blocks, respectively.

To handle this coarse-grained parallelization we developed a package of bash scripts able to distribute the concurrent jobs both on multiple nodes and multiple cores. Note that the number of jobs to be executed in parallel on different cores can be specifically tuned for each step of the P-SBAS processing chain depending on its characteristics in terms of RAM and CPU exploitation. In such a way we can optimize the use of the computing resources at disposal. Regarding them, in order to give a quantitative idea of the minimum requirements of the P-SBAS processing chain, we represent in Table 1 the average values of the percentage of used CPU, the maximum RAM occupation, the file system inputs (non cached reads in 512-byte blocks) and the file system outputs (non cached writes in 512-byte blocks) of a single job for each step of the P-SBAS chain (see Fig. 1). Moreover, we also specify if it is either a sequential or a parallel step. Note that within the steps exploiting multithreading programming we have values of CPU percent greater than 100 percent, indeed the percentage values are evaluated with respect to a single CPU.

The adopted strategy guarantees a wide applicability and results in a remarkable flexibility. Indeed, on the one hand, these scripts can run on any machine having a Linux Operating System and do not require any further software framework for the parallelization (i.e., Hadoop [80], Spark [81], Flink [82] etc.), which could add an overhead to the computation itself. On the other hand, such a solution allows us to easily set the distribution of the coarse-level parallel tasks of the processing on a multi-node, multi-core

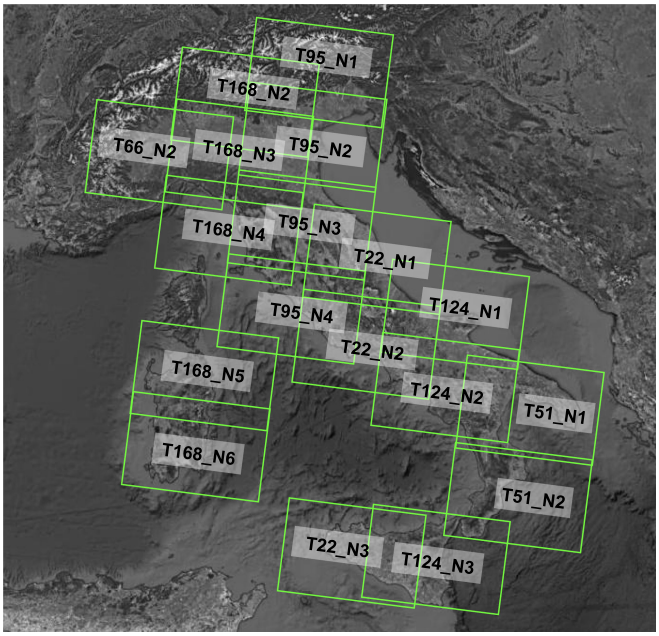

Fig. 2. Representation of the S1 slices acquired from descending orbits and processed through the S1 P-SBAS processing chain implemented within the AWS environment.

or hybrid multi-node/multi-core basis. This turned out to be very important in terms of robustness within diverse CC environments, where the computing instances can be very different in terms of hardware characteristics (CPUs, RAM, storage disks, network). Therefore, keeping the maximum flexibility in the way of managing the parallel tasks results in a maximization of the achieved scalability.

Actually, the multi-node implementation of the P-SBAS processing chain requires the computing nodes to be configured within a proper architecture. The followed strategy consists in distributing data among different computing nodes and, at the same time, keeping these data visible and accessible by all of the nodes, according to the data-dependencies of the P-SBAS processing approach. This is accomplished by attaching a dedicated storage disk (typically an SSD with very high I/O performances) to each computing node, and by mutually connecting all the disks through a Network File System (NFS) protocol [83]. Moreover, a policy to properly distribute the data and the parallel jobs among the computing nodes, aimed at minimizing the network occupation, is exploited as well. Such an implementation was designed to maximize the scalable performances of the P-SBAS processing chain in order to sustain its intensive I/O workload and has been thoroughly discussed in [69].

Finally, regarding the storage of the interferometric products generated by the P-SBAS algorithm, we leveraged the S3 storage where we created a bucket, i.e., a specific folder, in which as soon as a S1 P-SBAS processing run is completed, all the relevant results are uploaded for long-term preservation.

It is worth noting that the whole pipeline, including the download of the S1 input data from the S3 archive towards the computing nodes, the launch and the completion of the P-SBAS DInSAR processing chain and the transfer of the generated results to the S3 long-term storage, runs in a completely automatic way. We finally remark that the operations relevant to the transfer of data from/to the S3 storage are managed through Linux Bash scripts that use the Command Line Interface (CLI) commands, which allow handling all the AWS services from command line [84].

TABLE 2
Key Numbers of the P-SBAS Interferometric Analysis Performed over Italy (see Fig. 2)

PROCESSED SLICE	# S1 IWS SLC data and size [GB]	# Scenes after fusion	# Bursts and size [GB]	# Generated interferograms and size [GB]
T22_N1	#154	63	#2394	#173
	690 GB		320 GB	7.95 GB
T22_N2	#162	65	#2340	#180
	730 GB		311 GB	8.96 GB
T22_N3	#119	53	#1590	#144
	536 GB		210 GB	6.40 GB
T95_N1	#127	64	#1600	#176
	572 GB		215 GB	7.05 GB
T95_N2	#144	64	#1984	#176
	648 GB		265 GB	10.1 GB
T95_N3	#129	62	#1922	#167
	580 GB		256 GB	9.13 GB
T95_N4	#130	58	#1740	#157
	585 GB		233 GB	7.36 GB
T124_N1	#133	66	#1782	#181
	600 GB		240 GB	9.19 GB
T124_N2	#177	67	#2144	#184
	796 GB		289 GB	12.4 GB
T124_N3	#183	65	#1885	#176
	824 GB		254 GB	10.5 GB
T66_N1	#127	56	#1848	#155
	572 GB		251 GB	7.72 GB
T66_N2	#185	70	#2730	#194
	833 GB		370 GB	11.2 GB
T168_N2	#127	58	#1566	#161
	572 GB		213 GB	5.66 GB
T168_N3	#118	66	#1584	#182
	531 GB		216 GB	8.89 GB
T168_N4	#134	66	#2244	#183
	603 GB		305 GB	8.93 GB
T168_N5	#153	65	#1950	#180
	689 GB		266 GB	7.91 GB
T51_N1	#137	67	#2010	#185
	617 GB		280 GB	8.49 GB
T51_N2	#173	67	#2814	#185
	779 GB		392 GB	11.6 GB
Total	**#2,612**	**1,142**	**#35,605**	**#3,139**
	11,757 GB		**779 GB**	**779 GB**

4 Experimental Results

We present in this section the results of our national scale S1 P-SBAS DInSAR analysis carried out, through the AWS EC2 Cloud platform [66], on the Italian territory. In particular, for such an analysis, we processed 18 S1 slices, covering an overall area of more than 300,000 km^2, as shown in Fig. 2. We exploited in total 2,612 S1 IWS SLC images acquired from descending orbits within the time interval March 2015 – April 2017; the total number of S1 bursts involved in the analysis is 35,605.

Table 2 summarizes the key numbers of the performed processing. In particular, for each S1 processed slice, we specify in details the number of input S1 IWS SLC images, the number of scenes obtained after the fusion of the SLCs acquired in the same dates, the total number of processed

TABLE 3
CPU, RAM and I/O Exploitation for each Step of the P-SBAS Processing Chain

Step	seq/par /multi-th	% CPU	RAM (KB)	File System Input*	File System Output*
A	par	133	1,347,569	40,152,447	60,184,962
B	seq	94	1,441,600	1,483,294,680	1,888,794,624
C	par	99	854,762	0	2,750,468
D	par	187	4,808,590	56	1,087,666
E	par	116	2,312,053	270,601.94	1,946,894
F	par	101	1,106,064	1,487,766	2,548,521
G	par	216	1,413,130	11,737,541	5,465,632
H	par	100	1,420,391	1,871,313	106,416
I	par	113	578,865	140.81	287,144.97
J	par	118	10,418,773	5,255,053.36	12,620,487
K	multi-th	2,877	30,003,460	195,600	170,047,112
L	par/multi-th	655	73,630,428	2,345,654	21,347,763
M	seq	1,348	17,108,988	234,198,584	17,337,640
N	par/multi-th	98	48,968	0	6,112
O	seq	785	18,409,376	96,288	54,411,336

The T22_N1 S1 slice has been considered as a benchmark.
**Note that the file system inputs and the file system outputs are evaluated as non cached reads in 512-byte blocks and non cached writes in 512-byte blocks, respectively.*

TABLE 4
Adopted Coarse-Grained Parallelization Strategy (n. of Jobs Performed in Parallel for each Step of the P-SBAS Algorithm) and Overall CPU, RAM, I/O Exploitation Relevant to the T22_N1 Slice Processing Considered as a Benchmark

Step	seq/par/ multi-th	par jobs per node	% CPU	RAM (KB)	File System Input*	File System Output*
A	par	40	5,320	53,902,760	40,152,447	60,184,962
B	seq	/	94	1,441,600	1,483,294,680	1,888,794,624
C	par	64	6,330	37,162,240	0	176,029,952
D	par	33	6,170	158,683,470	1,848	135,892,978
E	par	54	6,250	124,850,862	14,612,454	105,132,276
F	par	60	6,060	66,363,840	89,265,960	152,911,260
G	par	29	6,260	40,980,770	340,388,689	158,503,328
H	par	60	6,000	85,223,460	112,278,780	6,384,960
I	par	55	6,200	31,837,575	7,700	15,792,920
J	par	47	5,540	489,682,331	246,987,491	593,162,889
K	multi-th	/	2,877	30,003,460	195,600	170,047,112
L	par/multi-th	7	4,580	500,412,996	16,419,578	149,434,341
M	seq	/	1,350	17,108,988	234,198,584	17,337,640
N	par/multi-th	60	5,880	2,938,080	0	366,720
O	seq	/	785	18,409,376	96,288	54,411,336

**Note that the file system inputs and the file system outputs are evaluated as non cached reads in 512-byte blocks and non cached writes in 512-byte blocks, respectively.*

bursts and generated interferograms. Moreover, for each one of these datasets, we also pointed out the corresponding size expressed in GigaByte (in red) to give an idea of the volume of data handled during the overall processing.

Concerning the selection of the AWS computing resources, as well as of the scheduling policy adopted for this large-scale P-SBAS processing, we leveraged the considerations that have been drawn in the previous section. In particular, since the AWS EC2 platform makes available a large range of instance typologies (with computing nodes having also a very large number of CPUs and high performing internal storage disks [78]) we had no severe constraints imposed by hardware configurations. Accordingly, there were two different possibilities for carrying out the P-SBAS processing of each S1 slice. The former was to split the parallel processes among different computing nodes (and, possibly, on their cores); in this case we would have exploited many AWS instances with medium performances in terms of number of CPUs, RAM and storage disk, and with a medium price. The latter was to use a single, highly performing instance equipped with several CPUs, a large RAM, as well as large internal Solid-State Drive (SSD) disks; this could allow us to distribute the parallel processes at a core level. The significant difference between the multi-node and multi-core scheduling policies lies in the fact that in the first case the use of the network is needed to transfer data among different nodes (even if in an optimized way), whereas in the second one this does not occur. We opted in this work for the second option, splitting the parallel processes of the P-SBAS processing of each S1 slice on different CPUs and exploiting the SSD shared storage able to sustain the I/O workload of the several processes reading and writing concurrently. Moreover, this choice allows us to exploit multiple nodes to carry out the processing of more S1 slices in parallel, thus significantly speeding up the whole processing.

In particular, we exploited for the P-SBAS processing of each S1 slice the i3.16xlarge instance, which is equipped with 64 vCPUs, 488 GiB of RAM and 8 SSD disks that we put into a RAID 0 configuration for a total of 15.2 TB of storage with an extremely high I/O bandwidth. For each step of the P-SBAS processing chain we defined the number of threads to be launched in parallel according to their average RAM and CPU exploitation in order to optimize the usage of the available CPUs. For the sake of clarity, in Table 3, we consider the T22_N1 S1 slice, which can be considered as a benchmark in terms of number of processed images and bursts, and we indicate, for each step of the P-SBAS processing chain, the maximum RAM occupation (KB), the percentage of used CPU, the file system inputs (non cached reads in 512-byte blocks) and the file system outputs (non cached writes in 512-byte blocks) of each single job. Note that such values were calculated as an average on the totality of the parallel jobs launched for each step. Moreover, in Table 4 we represent for each parallel step of the P-SBAS processing chain the number of jobs that we launched in parallel on the i3.16xlarge instance, with the corresponding values of total percentage of used CPU, the overall maximum RAM set size (KB) and the total number of file system inputs and outputs.

TABLE 5
Processing Times of the Overall S1 Slices

PROCESSED SLICE	Time [hours]	PROCESSED SLICE	Time [hours]
T22_N1	18.88	T124_N3	23.05
T22_N2	19.53	T66_N1	15.55
T22_N3	11.00	T66_N2	23.75
T95_N1	14.23	T168_N2	15.68
T95_N2	17.18	T168_N3	14.46
T95_N3	12.51	T168_N4	22.93
T95_N4	13.13	T168_N5	15.11
T124_N1	20.33	T51_N1	15.65
T124_N2	23.85	T51_N2	24.73
Average time ~18 hours			

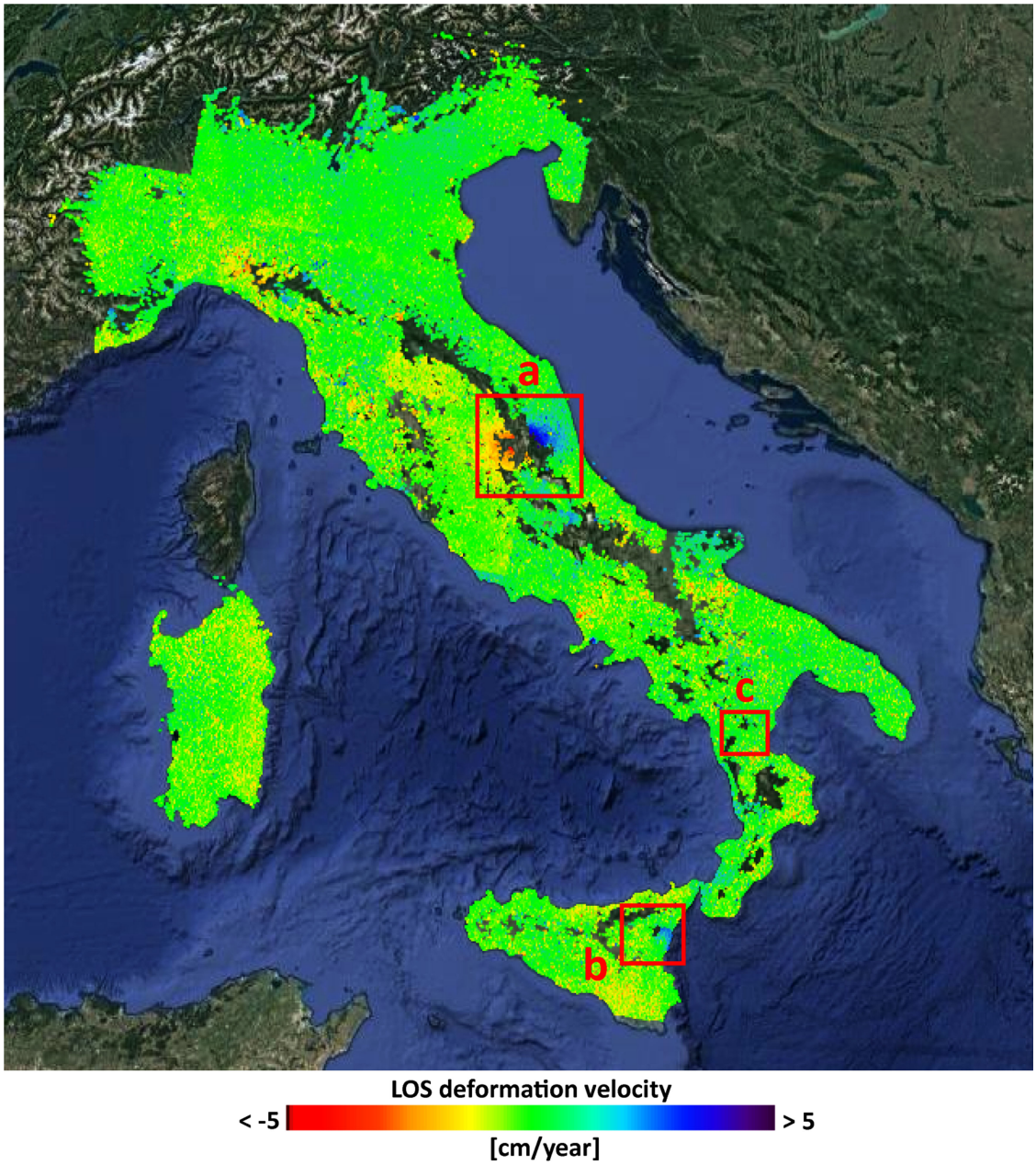

Fig. 3. Overall mean deformation velocity map of the Italian territory generated through the S1 P-SBAS processing chain implemented within the AWS environment. The red rectangles represent three areas characterized by significant deformation phenomena: (a) the Central Italy area interested by the seismic sequence occurred between August 2016—October 2016, (b) the Mt. Etna Volcano, and (c) the little town of Plataci (southern Italy) affected by an extended landslide. The deformation phenomena relevant to these three areas are investigated in more details in Fig. 4

It is worth underlying that the rationale adopted for the implemented parallelization comes from the studies on the scalability of the P-SBAS approach, which have been thoroughly discussed in [67], [68], [69]; accordingly, an extensive scalability analysis is here omitted for brevity but can be found in the available literature on this topic [67], [68], [69]. Moreover, as it is clear from Table 4, the proposed strategy allows us to fully exploit the computing resources (CPUs, RAM and I/O) in the majority of the parallel steps of the processing chain, thus achieving very satisfactory processing times. They are represented in Table 5 for all the considered S1 slices and vary depending on the size of the input data of the processing, i.e., the initial dataset, the number of processed bursts, the generated interferograms and also on the backscattering properties of the scene observed by the sensor that dictate the number of coherent points in input to the PhU procedure. Note that the shortest processing lasted 11 hours, whereas the longest one took a little more than 24 hours to complete. We further remark that, on average, the processing of a S1 slice lasts approximately 18 hours, thus suggesting that the overall analysis can be performed within one day by exploiting, in parallel, 18 i3.16xlarge AWS instances, with a cost of less than 1800 USD if on-demand instances are used.

Fig. 3 shows the overall mean deformation velocity map obtained by merging the 18 geocoded mean deformation velocity maps relevant to the considered S1 slices, computed with a spacing of about 80×80 m^2. According to the color bar depicted in the figure, green color represents areas that are stable in terms of surface displacements, whereas the red and blue colors stand for negative and positive deformation

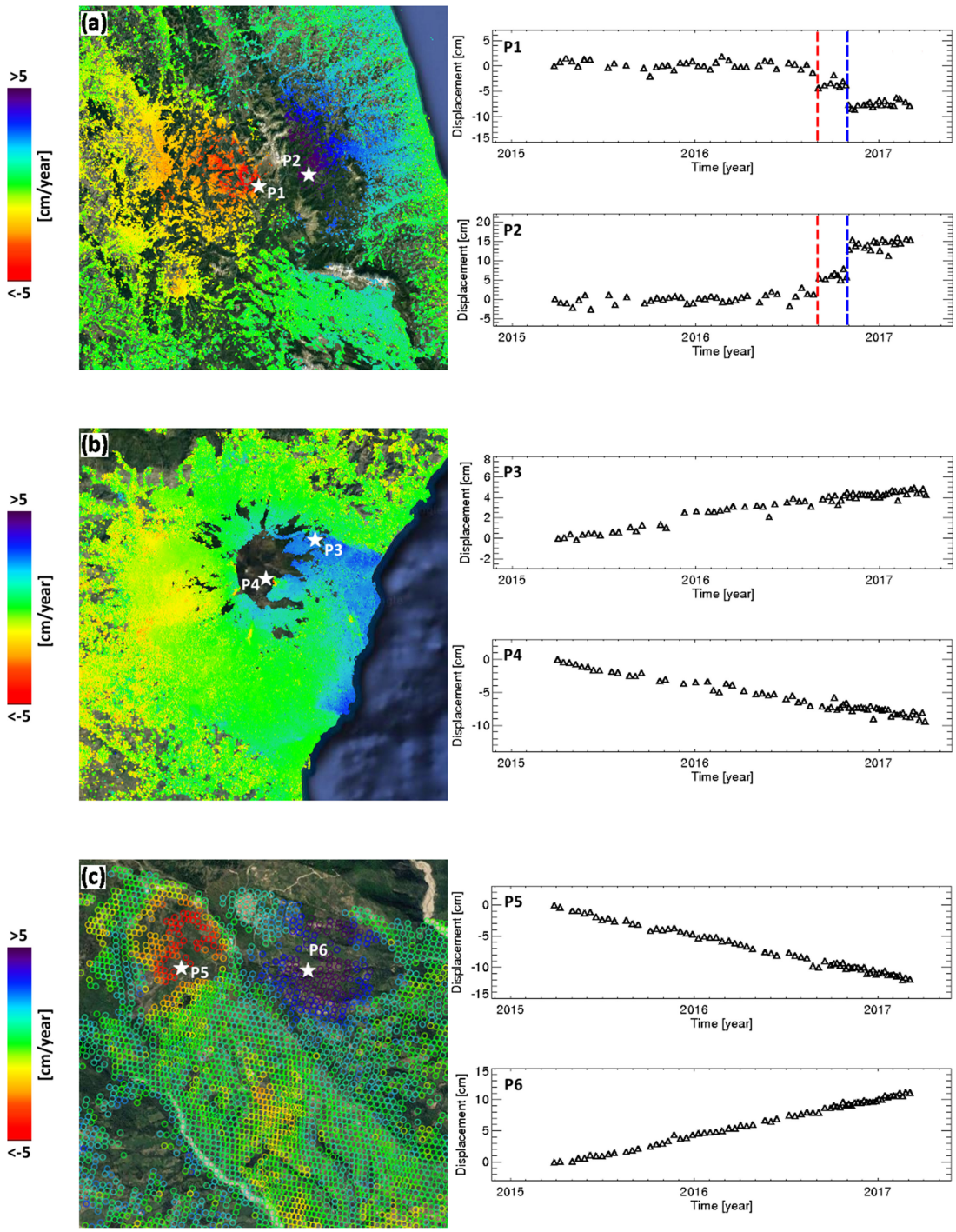

Fig. 4. (Left) Zoomed views of the three areas identified in Fig. 3 by the red rectangles labeled as (a), (b) and (c). (Right) LOS-projected displacement time series relevant to pixels, marked by the white stars in the maps, located in the maximum deforming areas. (a) Mean deformation velocity map related to the 2016 seismic sequence occurred in Central Italy. The deformation time series of two pixels (labeled as P1 and P2) located in the maximum displacement area of the co-seismic signals are also depicted. Note that the vertical dashed lines indicate the two main seismic events of Amatrice and Visso/Norcia. (b) Mean deformation velocity map of the Mt. Etna volcano and displacement time series of two pixels, located in correspondence to the southern side of the Pernicana Fault System (labeled as P3) and to the Valle del Bove area (labeled as P4). (c) Mean deformation velocity map associated to the extended slope movements affecting the little town of Plataci (southern Italy) and corresponding time series of displacement for two pixels located in the maximum deformation areas on the opposite mountainsides, labeled as P5 and P6, respectively.

velocity values, which correspond to an increase and decrease of the LOS sensor-to-target distance, respectively. Moreover, in Fig. 3, we highlight three zones particularly relevant from the deformation viewpoint, which are delineated by the red rectangles (a), (b) and (c), and are zoomed in Fig. 4. In particular, in Fig. 4a we report a sketch of the mean deformation velocity map relevant to Central Italy. It is evident a deformation pattern characterized by a very large extent, which is associated to the seismic sequence that struck Central Italy in 2016. Moreover, Fig. 4a highlights the presence of two lobes, characterized by both negative and positive LOS-projected displacement signals, respectively, which reveal a complex SW-NE oriented deformation pattern [86], [87]. Furthermore, we report the displacement time series relevant

to two pixels (labeled as P1 and P2 in Fig. 4a and marked by white stars), located in the maximum co-seismic deformation area. They clearly show the LOS-projected deformation signal associated to the occurred seismic sequence (see the red and blue vertical dashed lines that identify both the Amatrice [86] and Visso/Norcia [87] events).

Fig. 4b depicts a zoomed view of the mean deformation velocity map of Fig. 3 relevant to the Mt. Etna volcano. This map shows the complex ground deformation scenario involving the entire volcanic edifice and related to magmatic inflation/deflation, differential motion across fault systems, as well as local subsidence [88], [89]. In particular, we focus on the northern border of the volcano, bounded by the Pernicana Fault System (PFS), where a strong deformation signal of the eastern flank is clearly evident. The velocity map shows a decreasing sensor-to-target distance (i.e., positive displacement), as testified by the plot of the deformation time series related to a pixel located in the PFS southern side (identified by a white star in Fig. 4b and labeled as P3). The map in Fig. 4b also reveals the presence of a localized subsidence, characterized by a deformation rate of about 5 cm/year, related to lava flow compaction within the Valle del Bove area (see the temporal evolution of the deformation reported for the pixel labeled as P4 and identified by a white star in Fig. 4b).

Finally, Fig. 4c shows a zoomed view of the map in Fig. 3, corresponding to the area surrounding the little town of Plataci (southern Italy), which is interested by extended landslide phenomena, affecting both the mountain slopes where Plataci is located [90]. The plots reported in Fig. 4c show the temporal evolution of the retrieved LOS-projected deformation, characterized by a cumulative displacement value that exceeds 10 cm for the whole period of observation, for two pixels located at the opposite mountainsides (see the white stars in Fig. 4c) and labeled as P5 and P6, respectively.

5 Discussion and Conclusions

EO data archives are expanding at an unprecedented speed, both in size and variety. Existing, new and even at design stage remote sensing sensors are and will be soon available, providing EO data characterized by enhanced spatial coverage and resolution, and high temporal acquisition rate. Furthermore, the computing power is growing in parallel, allowing us to process such data at a global scale. This scenario represents a unique opportunity to boost the study and the knowledge of the Earth System dynamics. Indeed, the joint exploitation of huge data archives and computing resources paves the way to a new approach to science based on data-intensive exploration and analysis, which is responsible for a real revolution within the known science paradigms [2], [3].

In this paper we presented a CC based pipeline for carrying out national scale interferometric analyses from large multitemporal SAR datasets acquired by the Sentinel-1 constellation. Our DInSAR processing chain implements the P-SBAS approach [60] in order to generate time series and mean velocity maps relevant to Earth's surface deformation processes. We dealt with the main relevant issues of Big Data processing, including also the storage of both the input SAR images and the generated interferometric value added products.

As a matter of fact, as datasets grow, the most efficient way to process them is to move the computation as close to the data itself as possible. This is the reason why we built a S1 SLC images archive, containing all the S1 data acquired over Italy, continuously updated and publicly available, in the AWS S3 storage [66], from which the input data are directly transferred to the AWS EC2 computing instances exploited for their processing. In particular, we developed a complete pipeline within the AWS environment addressing the download of the S1 input data from the created S3 archive towards the EC2 [78] computing nodes, the run of the P-SBAS DInSAR processing, which is carried out in parallel, and, finally, the transfer of the obtained results again to the S3 long-term storage. It is worth noting that all the described actions are performed in an automatic way.

As experimental results we presented a national-scale DInSAR analysis accomplished over the Italian territory by processing 2612 S1 IWS SLC data (the overall dataset size is 11,757 GB) acquired from descending orbits within the March 2015—April 2017 time span. In particular, we produced the mean surface deformation velocity map of the whole Italian peninsula with a spatial resolution of about $80 \times 80\mathrm{m}^2$ and, for each pixel of this map, we retrieved the time series representing the evolution of the surface deformation within the considered time interval. The generated interferometric products clearly identify several deformation phenomena due to different sources. It is, for example, clearly visible the deformation pattern due to the earthquakes occurred in Central Italy between August 2016 and October 2016. Moreover, the deformation phenomena affecting the Mt. Etna volcano and an extended landslide, close to the little town of Plataci (southern Italy), are shown as key examples.

The presented CC based DInSAR processing chain addresses four relevant aspects of the Big Data framework that, according to the Vs definition of Laney [59], are: Volume, Velocity, Value and Veracity. It is, indeed, envisaged to process large Volumes of data in short time frames (Velocity); in fact, the presented national scale interferometric analysis can be performed by exploiting in parallel 18 AWS i3.16xlarge instances, within one day and with a cost of less than 1800 USD.

Additionally, the generated products, i.e., the deformation time series and maps, intrinsically hold Value and Veracity. Indeed, on the one hand, they are value added data containing a precise physical information extracted from the input SAR data; on the other hand, they are characterized by documented quality and uncertainty. In particular, the achieved measurement accuracy (from centimeter to millimeter) has been proven in several studies [42], [43]. Moreover, we provide the information about the deformation only in the pixels of the scene in which it can be considered reliable [76].

A very relevant further development regards the implementation of the presented CC solution within environments devoted to the dissemination, sharing and maximization of the EO data exploitation within the worldwide scientific community. There are some platforms, both already existing and under development, pursuing these goals; this is for example the case of the ESA GPOD [61] and GEP [62], as well as the EPOSAR service within the European Plate Observing System (EPOS) Research Infrastructure [85].

Such a kind of environments are, indeed, addressed to exploit Cloud Computing resources that can be accessed as Web Services; furthermore, they are intended to make available any kind of data, like those acquired by different EO satellites, GPS and in situ measurements, thus covering also the Variety aspect of the Big Data paradigm. Finally they offer tools for the query, the interoperability and the Visualization of all these kinds of data. Within this framework the proposed S1 P-SBAS processing chain may become a very effective tool for:

- allowing any scientific user to carry out his own DInSAR analysis over an area of interest;
- accessing/downloading/visualizing/sharing value added interferometric products that are themselves useful both for monitoring and research purposes but that can be also used as input for further analyses;
- jointly exploiting the generated results with other kinds of data, like GPS measurements, global atmospheric reanalysis data, in situ measurements, etc., in order to obtain further innovative products.

In conclusion, the proposed CC based P-SBAS processing chain, together with the presented results, clearly demonstrate how the joint exploitation of advanced remote sensing methodologies and new ICT technologies can be essential for data intensive scientific exploration, thus paving the way to innovative methods and new approaches to science.

Acknowledgments

This work was supported by the Italian Civil Defense Protection Department, the ESA's GEP project, the EPOS-IP project of the European Union Horizon 2020 for research and innovation program (grant agreement 676564), the EOSC-hub project of the European Union Horizon 2020 for research and innovation program (grant agreement 777536), the I-AMICA (PONa3_00363) project, and the IREA-CNR/Italian Ministry of Economic Development DGS-UNMIG agreement. Sentinel-1 SAR data are copyright of Copernicus (2016); the DEMs of the Italian territory are acquired through the SRTM archive.

References

[1] C. R. Sugimoto, H. R. Ekbia, and M. Mattioli, "Big data and science," in *Big Data Is Not a Monolith*, 1. Cambridge, MA, USA: MIT Press, 2016.

[2] T. Hey, S. Tansley, and K. Tolle, "The fourth paradigm: Data-intensive scientific discovery," Redmond, WA, USA: Microsoft Research, 2009.

[3] G. Bell, T. Hey, and A. Szalay, "Beyond the data deluge," *Sci.*, vol. 323, no. 5919, pp. 1297–1298, 2009, doi: 10.1126/science.1170411

[4] A. Eldawy and M. F. Mokbel, "The era of big spatial data: A survey," in *The Era of Big Spatial Data: A Survey*. Breda, Netherlands: Now Publishers Inc., Dec. 2016, pp. 163–273, http://dx.doi.org/10.1561/1900000054

[5] O. B. Sezer, E. Dogdu, and A. M. Ozbayoglu, "Context-aware computing, learning, and big data in internet of things: A survey," *IEEE Internet Things J.*, vol. 5, no. 1, pp. 1–27, Feb. 2018.

[6] B. M. Mathisen, L. W. M. Weinhofen, and D. Roman, "Empirical big data research: A systematic literature mapping," *Springer J. Data Sci. Eng.*, arXiv:1509.03045, Sep. 2015.

[7] P. P. Mathieu, et al., "The ESA's earth observation open science program [space agencies]," *IEEE Geosci. Remote Sens. Mag.*, vol. 5, no. 2, pp. 86–96, Jun. 2017.

[8] M. Chi, A. Plaza, J. A. Benediktsson, Z. Sun, J. Shen, and Y. Zhu, "Big data for remote sensing: Challenges and opportunities" *Proc. IEEE*, vol. 104, no. 11, pp. 2207–2219, Nov. 2016.

[9] D. Massonnet, M. Rossi, C. Carmona, F. Adragna, G. Peltzer, K. Feigl, and T. Rabaute, "The displacement field of the Landers earthquake mapped by radar interferometry," *Nature*, vol. 364, no. 6433, pp. 138–142, Jul. 1993.

[10] G. Peltzer and P. A. Rosen, "Surface displacement of the 17 May 1993 Eureka Valley earthquake observed by SAR interferometry," *Sci.*, vol. 268, no. 5215, pp. 1333–1336, Jun. 1995.

[11] M. A. Chinnery, "The deformation of the ground around surface faults," *Bull. Seismol. Soc. Am.*, vol. 51, pp. 355–372, Jul. 1961.

[12] D. Massonnet, P. Briole, and A. Arnaud, "Deflation of Mount Etna monitored by spaceborne radar interferometry," *Nature*, vol. 375, no. 6532, pp. 567–570, Jun. 1995.

[13] K. Mogi, "Relations between the eruptions of various volcanoes and the deformations of the ground surfaces around them," *Bull. Earthquake Res. Instit.*, vol. 36, pp. 99–134, 1958.

[14] R. Lanari, G. De Natale, P. Berardino, E. Sansosti, G. P. Ricciardi, S. Borgstrom, P. Capuano, F. Pingue, and C. Troise, "Evidence for a peculiar style of ground deformation inferred at Vesuvius volcano," *Geophys. Res. Lett.*, vol. 29, no. 9, pp. 6-1–6-4, 2002, doi: 10.1029/2001GL014571

[15] L. Cascini, S. Ferlisi, G. Fornaro, R. Lanari, D. Peduto, and G. Zeni, "Subsidence monitoring in Sarno urban area via multi-temporal DInSAR technique," *Int. J. Remote Sens.*, vol. 27, no. 8, pp. 1709–1716, 2006.

[16] C. Colesanti and J. Wasowski, "Investigating landslides with space-borne synthetic aperture radar (SAR) interferometry," *Eng. Geology*, vol 88, pp. 173–199, 2006.

[17] M. Manzo, G. P. Ricciardi, F. Casu, G. Ventura, G. Zeni, S. Borgström, P. Berardino, C. Del Gaudio, and R. Lanari, "Surface deformation analysis in the Ischia island (Italy) based on space-borne radar interferometry," *J. Volcanology Geothermal Res.*, vol. 151, pp. 399–416, 2006, doi: 10.1016/j.jvolgeores.2005.09.010.

[18] W. E. Farrell, "Deformation of the Earth by surface loads," *Rev. Geophys.*, vol. 10, no. 3, pp. 761–797, Aug. 1972.

[19] P. A. Hsieh, "Deformation-induced changes in hydraulic head during ground-water withdrawal," *Groundwater*, vol. 34, pp. 1082–1089, 1996.

[20] R. F. Yerkes and R. O. Castle, "Surface deformation associated with oil and gas field operations in the United States," in *Proc. Tokyo Symp. Land Subsidence*, 1969, pp. 55–66. [Online]. Available: pubs.rsc.org

[21] F. M. Orr Jr., "CO 2 capture and storage: Are we ready?," *Energy Environ. Sci.*, vol. 2, pp. 449–458, 2009.

[22] S. Rackley. "Carbon capture and storage". [Online]. Available: https://books.google.com, 2009.

[23] M. P. O' Reilly and B. M. New, "New settlements above tunnels in the United Kingdom-their magnitude and prediction," *Publ.: Instit. Mining. Metallurgy*. [Online]. Available: https://trid.trb.org, 1982.

[24] N. Gourmelen, F. Amelung, F. Casu, M. Manzo, and R. Lanari, "Mining-related ground deformation in Crescent Valley, Nevada: Implications for sparse GPS networks," *Geophys. Res. Lett.*, vol. 34, no. 9, May 2007, Art. no. L09309, doi: 10.1029/2007GL029427

[25] R. W. Clough and R. J. Woodward, "Analysis of embankment stresses and deformations," *J. Soil Mech. Found. Div.*, vol. 93, pp. 529–549, 1967.

[26] R. M. Goldstein, H. A. Zebker, and C. L. Werner, "Satellite radar interferometry: Two-dimensional phase unwrapping," *Radio Sci.*, vol. 23, no. 4, pp. 713–720, Jul./Aug. 1988.

[27] D. Massonnet and K. L. Feigl, "Radar interferometry and its application to changes in the Earth's surface," *Rev. Geophys.*, vol. 36, pp. 441–500, 1998.

[28] R. Burgmann, P. A. Rosen, and E. J. Fielding, "Synthetic aperture radar interferometry to measure Earth's surface topography and its deformation," *Annu. Rev. Earth Planet Sci.*, vol. 28, pp. 169–209, May 2000.

[29] A. K. Gabriel, R. M. Goldstein, and H. A. Zebker, "Mapping small elevation changes over large areas: Differential radar interferometry," *J. Geophys. Res.*, vol. 94, no. B7, pp. 9183–9191, Jan. 1989.

[30] P. A. Rosen, S. Hensley, I. R. Joughin, F. K. Li, S. N. Madsen, E. Rodriguez, and R. M. Goldstein, "Synthetic aperture radar interferometry," *Proc. IEEE*, vol. 88, no. 3, pp. 333–382, Mar. 2000.

[31] G. Franceschetti and R. Lanari, *Synthetic Aperture Radar Processing*. Boca Raton, FL, USA: CRC Press, 1999.
[32] H. A. Zebker and J. Villasenor, "Decorrelation in interferometric radar echoes," *IEEE Trans. Geosci. Remote Sens.*, vol. 30, no. 5, pp. 950–959, Sep. 1992.
[33] Y. Fialko, M. Simons, and D. Agnew, "The complete (3-D) surface displacement field in the epicentral area of the 1999 Mw 7.1 Hector Mine earthquake, California, from space geodetic observations," *Geophys. Res. Lett.*, vol. 28, pp. 3063–3066, Aug. 2001.
[34] A. Ferretti, C. Prati, and F. Rocca, "Permanent scatterers in SAR interferometry," *IEEE Trans. Geosci. Remote Sens.*, vol. 39, no. 1, pp. 8–20, Jan. 2001.
[35] C. Werner, U. Wegmüller, T. Strozzi, and A. Wiesmann, "Interferometric point target analysis for deformation mapping," in *Proc. IEEE Int. Geosci. Remote Sens. Symp.*, vol. 7, pp. 4362–4364, 2003.
[36] A. Hooper, H. Zebker, P. Segall, and B. Kampes, "A new method for measuring deformation on volcanoes and other natural terrains using InSAR persistent scatterers," *Geophys. Res. Lett.*, vol. 31, no. 23, Dec. 2004, Art. no. L23611.
[37] P. Berardino, G. Fornaro, R. Lanari, and E. Sansosti, "A new algorithm for surface deformation monitoring based on small baseline differential SAR interferograms," *IEEE Trans. Geosci. Remote Sens.*, vol. 40, no. 11, pp. 2375–2383, Nov. 2002.
[38] R. Lanari, O. Mora, M. Manunta, J. J. Mallorquì, P. Berardino, and E. Sansosti, "A small-baseline approach for investigating deformations on full-resolution differential SAR interferograms," *IEEE Trans. Geosci. Remote Sens.*, vol. 42, no. 7, pp. 1377–1386, Jul. 2004.
[39] A. Hooper, "A multi-temporal InSAR method incorporating both persistent scatterer and small baseline approaches," *Geophys. Res. Lett.*, vol. 35, no. 16, Aug. 2008, Art. no. L16 302.
[40] A. Ferretti, A. Fumagalli, F. Novali, C. Prati, F. Rocca, and A. Rucci, "A new algorithm for processing interferometric data-stacks: SqueeSAR," *IEEE Trans. Geosci. Remote Sens.*, vol. 49, no. 9, pp. 3460–3470, Sep. 2011.
[41] E. Sansosti, P. Berardino, M. Bonano, F. Calo', R. Castaldo, F. Casu, M. Manunta, M. Manzo, A. Pepe, S. Pepe, G. Solaro, P. Tizzani, G. Zeni, and R. Lanari, "How second generation SAR systems are impacting the analysis of ground deformation," *Int. J. Appl. Earth Obs. Geoinf.*, vol. 28, pp. 1–11, 2014. doi: 10.1016/j.jag.2013.10.007
[42] F. Casu, M. Manzo, and R. Lanari, "A quantitative assessment of the SBAS algorithm performance for surface deformation retrieval from DInSAR data," *Remote Sens. Environ.*, vol. 102, no. 3/4, pp. 195–210, Jun. 2006.
[43] M. Bonano, M. Manunta, A. Pepe, L. Paglia, and R. Lanari, "From previous C-Band to New X-Band SAR systems: Assessment of the DInSAR mapping improvement for deformation time-series retrieval in urban areas," *IEEE Trans Geosci Remote Sens*, vol. 51, no. 4, pp. 1973–1984, Apr. 2013.
[44] L. D'Auria, S. Pepe, R. Castaldo, F. Giudicepietro, G. Macedonio, P. Ricciolino, P. Tizzani, F. Casu, R. Lanari, M. Manzo, M. Martini, E. Sansosti, and I. Zinno, "Magma injection beneath the urban area of Naples: A new mechanism for the 2012-2013 volcanic unrest at Campi Flegrei caldera," *Sci. Rep.*, vol. 5, 2015, Art. no. 13100. doi: 10.1038/srep13100
[45] J. Fernández, P. Tizzani, M. Manzo, A. Borgia, P. J. González, J. Martí, A. Pepe, A. G. Camacho, F. Casu, P. Berardino, J. F. Prieto, and R. Lanari, "Gravity-driven deformation of Tenerife measured by InSAR time series analysis," *Geophys. Res. Lett.*, vol. 36, no. 4, p. 306, 2009, doi: 10.1029/2008GL036920.
[46] F. Diao, T. R. Walter, G. Solaro, R. Wang, M. Bonano, M. Manzo, S. Ergintav, Y. Zheng, X. Xiong, and R. Lanari, "Fault locking near Istanbul: Indication of earthquake potential from InSAR and GPS observations," *Geophys. J. Int.*, vol. 205, 490–498, 2016.
[47] M. Manzo, Y. Fialko, F. Casu, A. Pepe, and R. Lanari, "A quantitative assessment of DInSAR measurements of interseismic deformation: The southern san andreas fault case study," *Pure Appl. Geophys*, vol. 169, no. 2012, pp: 1463–1482, 2011, https://doi.org/10.1007/s00024-011-0403-2
[48] R. Lanari, P. Berardino, M. Bonano, F. Casu, A. Manconi, M. Manunta, M. Manzo, A. Pepe, S. Pepe, E. Sansosti, G. Solaro, P. Tizzani, and G. Zeni, "Surface displacements associated with the L'Aquila 2009 Mw 63 earthquake Central Italy: New evidence from DInSAR time series analysis," *Geophys Res. Letter*, vol. 37, 2010, Art. no. L20309, doi: 101029/2010GL044780
[49] F. Calò, F. Ardizzone, R. Castaldo, P. Lollino, P. Tizzani, F. Guzzetti, R. Lanari, M. Angeli, F. Pontoni, and M. Manunta, "Enhanced landslide investigations through advanced DInSAR techniques: The Ivancich case study, Assisi, Italy," *Remote Sens. Environ.*, vol. 142, pp. 69–82, 2014.
[50] M. Cignetti, A. Manconi, M. Manunta, D. Giordan, C. De Luca, P. Allasia, and F. Ardizzone, "Taking advantage of the ESA G-POD service to study ground deformation processes in high mountain areas: A Valle d'Aosta case study, Northern Italy," *Remote Sens.*, vol. 8, no. 10, p. 852, 2016, doi: 10.3390/rs8100852.
[51] M. Bonano, M. Manzo, F. Casu, M. Manunta, and R. Lanari, "DInSAR for the monitoring of cultural heritage sites," in *Sensing the Past. Geoscience and Sensing Technologies for Cultural Heritage*. N. Masini, F. Soldovieri (eds)., Cham Switzerland: Springer, pp 117–134, Chapter 6, 2016.
[52] L. Solari, A. Ciampalini, F. Raspini, S. Bianchini, I. Zinno, M. Bonano, M. Manunta, S. Moretti, and N. Casagli, "Combined use of C-and X-Band SAR data for subsidence monitoring in an urban area," *Geosciences*, vol. 7, no. 2, 2017, Art. no. 21, doi: 10.3390/geosciences7020021
[53] S. Scifoni, M. Bonano, M. Marsella, A. Sonnessa, V. Tagliafierro, M. Manunta, R. Lanari, C. Ojha, and M. Sciotti, "On the joint exploitation of long-term DInSAR time series and geological information for the investigation of ground settlements in the town of Roma (Italy)," *Remote Sens. Environ.*, vol. 182, pp. 113–127, 2016.
[54] M. Manunta, M. Marsella, G. Zeni, M. Sciotti, S. Atzori, and R. Lanari, "Two-scale surface deformation analysis using the SBAS-DInSAR technique: A case study of the city of Rome, Italy," *Int. J. Remote Sens.*, vol. 29, no. 6, pp. 1665–1684, 2008.
[55] A. Pepe, E. Sansosti, P. Berardino, and R. Lanari, "On the generation of ERS/ENVISAT DInSAR time-series via the SBAS technique," *IEEE Geosci. Remote Sens. Letters*, vol. 2, no. 3, pp. 265–269, Jul. 2005.
[56] M. Bonano, M. Manunta, M. Marsella, and R. Lanari, "Long-term ERS/ENVISAT deformation time-series generation at full spatial resolution via the extended SBAS technique," *Int. J. Remote Sens.*, vol. 33, pp. 4756–4783, 2012.
[57] R. Torres, P. Snoeij, D. Geudtner, D. Bibby, M. Davidson, E. Attema, P. Potin, B. Rommen, N. Floury, M. Brown, I. Traver, P. Deghaye, B. Duesmann, B. Rosich, N. Miranda, C. Bruno, M. L'Abbate, R. Croci, A. Pietropaolo, M. Huchler, and F. Rostan, "GMES Sentinel-1 mission," *Remote Sens. Environ.*, vol. 120, pp. 9–24, 2012.
[58] F. De Zan and A. M. Monti Guarnieri, "TOPSAR: Terrain observation by progressive scans," *IEEE Trans. Geosci. Remote Sens.*, vol. 44, no. 9, pp. 2352–2360, Sep. 2006.
[59] D. Laney, "3-D data management: Controlling data volume, velocity and variety," *Application Delivery Strategies* by META Group Inc. Retrieved from http://blogs.gartner.com/doug-laney/files/2012/01/ad949-3D-Data-Management-Controlling-DataVolumeVelocityandVariety.pdf, 2001.
[60] F. Casu, S. Elefante, P. Imperatore, I. Zinno, M. Manunta, C. De Luca, and R. Lanari, "SBAS-DInSAR parallel processing for deformation time-series computation," *IEEE J. Sel. Top. Appl. Earth Obs. Remote Sens.*, vol. 7, no. 8, pp. 3285–3296, Aug. 2014.
[61] ESA Grid Processing on Demand. [Online]. Available: https://gpod.eo.esa.int
[62] The Geohazard Exploitation Platform and Portal [Online]. Available: https://geohazards-tep.eo.esa.int/#!pages/initiative
[63] C. De Luca, R. Cuccu, S. Elefante, I. Zinno, M. Manunta, V. Casola, G. Rivolta, R. Lanari, and F. Casu, "An on-demand web tool for the unsupervised retrieval of Earth's surface deformation from SAR data: The P-SBAS service within the ESA G-POD environment," *Remote Sens.*, vol. 7, no. 11, pp. 15630–15650, 2015, doi: 10.3390/rs71115630
[64] S. Nepal and S. Pandey, "Guest editorial: Cloud computing and scientific applications (CCSA)—big data analysis in the cloud," *Comput. J.*, vol. 59, no. 3, pp. 285–286, Mar. 2016.
[65] Amazon Web Services., 2015. [Online]. Available: https://aws.amazon.com/
[66] Amazon Web Services S3. [Online]. Available: https://aws.amazon.com/s3/?nc1.h_ls
[67] I. Zinno, S. Elefante, L. Mossucca, C. De Luca, M. Manunta, O. Terzo, R. Lanari, and F. Casu, "A first assessment of the P-SBAS DInSAR algorithm performances within a cloud computing environment," *IEEE J. Sel. Top. Appl. Earth Obs. Remote Sens.*, vol. 8, no. 10, pp. 4675–4686, Oct. 2015.

[68] I. Zinno, L. Mossucca, S. Elefante, C. De Luca, V. Casola, O. Terzo, F. Casu, and R. Lanari, "Cloud computing for Earth surface deformation analysis via spaceborne radar imaging: A case study," *IEEE Trans. Cloud Comput.*, vol. 4, no. 1, pp. 104–118, Jan.-Mar. 2016.
[69] I. Zinno, F. Casu, C. D. Luca, S. Elefante, R. Lanari, and M. Manunta, "A cloud computing solution for the efficient implementation of the P-SBAS DInSAR approach," *IEEE J. Sel. Top. Appl. Earth Obs. Remote Sens.*, vol. 10, no. 3, pp. 802–817, Mar. 2017.
[70] C. De Luca, I. Zinno, M. Manunta, R. Lanari, and F. Casu, "Large areas surface deformation analysis through a cloud computing P-SBAS approach for massive processing of DInSAR time series, *Remote Sens. Environ.*, vol. 202, pp. 3–17, ISSN 0034-4257, Dec. 2017.
[71] J. C. Curlander, and R. McDonough, *Synthetic Aperture Radar – System and Signal Processing*, New York, NY, USA: Wiley, 1991.
[72] E. Sansosti, P. Berardino, M. Manunta, F. Serafino, and G. Fornaro, "Geometrical SAR image registration," *IEEE Trans. Geosci. Remote Sens.*, vol. 44, no. 10, pp. 2861–2870, Oct. 2006.
[73] R. Scheiber and A. Moreira, "Coregistration of interferometric SAR images using spectral diversity," *IEEE Trans. Geosci. Remote Sens.*, vol. 38, no. 5, Sep. 2000.
[74] R. M. Goldstein and C. L. Werner, "Radar interferogram filtering for geophysical applications," *Geophys. Res. Lett.*, vol. 25, no. 21, pp. 4035–4038, Nov. 1998.
[75] I. Baran, M. P. Stewart, B. M. Kampes, Z. Persky, and P. Lilly, "A modification to the Goldstein radar interferogram filter," *IEEE Trans. Geosci. Remote Sens.*, vol. 41, no. 9, pp. 2114–2118, Sep. 2003.
[76] A. Pepe and R. Lanari, "On the extension of the minimum cost flow algorithm for phase unwrapping of multitemporal differential SAR interferograms," *IEEE Trans. Geosci. Remote Sens.*, vol. 44, no. 9, pp. 2374–2383, Sep. 2006.
[77] P. Imperatore, A. Pepe, and R. Lanari, "Multichannel phase unwrapping: Problem topology and dual-level parallel computational model," *IEEE Trans. Geosci. Remote Sens.*, vol. 53, no. 10, pp. 5774–5793, Oct. 2015.
[78] Amazon EC2. [Online]. Available: http://docs.aws.amazon.com/AWSEC2/latest/UserGuide/concepts.html
[79] Copernicus Open Access Hub. [Online] Available: https://scihub.copernicus.eu
[80] Apache Hadoop. [Online]. Available: http://hadoop.apache.org
[81] Apache Spark. [Online]. Available: https://spark.apache.org/sql/
[82] Apache Flink. [Online]. Available: https://flink.apache.org
[83] R. Sandberg, D. Goldberg, S. Kleiman, D. Walsh, and B. Lyon, "Design and Implementation of the SUN network filesystem," in *Proc. USENIX Conf.*, pp. 119–30, 1985.
[84] AWS Command Line Interface. [Online] Available: https://aws.amazon.com/cl
[85] EPOS- European Plate Observing System – A Research Infrastructure for Solid Earth Science. [Online]. Available: https://www.epos-ip.org
[86] G. Lavecchia, R. Castaldo, R. De Nardis, V. De Novellis, F. Ferrarini, S. Pepe, F. Brozzetti, G. Solaro, D. Cirillo, M. Bonano, P. Boncio, F. Casu, C. De Luca, R. Lanari, M. Manunta, M. Manzo, A. Pepe, I. Zinno, and P. Tizzani, "Ground deformation and source geometry of the 24 August 2016 Amatrice earthquake (Central Italy) investigated through analytical and numerical modeling of DInSAR measurements and strctural-geological data," *Geophys. Res. Lett.*, vol. 43, no. 12, pp. 389–398, 2016, doi:10.1002/2016GL071723
[87] D. Cheloni, et al., "Geodetic model of the 2016 Central Italy earthquake sequence inferred from InSAR and GPS data," *Geophys. Res. Lett.*, vol. 44, pp. 6778–6787, 2017, doi: 10.1002/2017GL073580
[88] G. Solaro, V. Acocella, S. Pepe, J. Ruch, M. Neri, and E. Sansosti, "Anatomy of an unstable volcano through InSAR observations from 1994 to 2008: Multiple processes affecting flank instability at Mt. Etna," *J. Geophys. Res.*, vol. 115, 2010, Art. no. B10405, doi: 10.1029/2009JB000820
[89] J. Ruch, , S. Pepe, F. Casu, V. Acocella, M. Neri, G. Solaro, and E. Sansosti, "How do volcanic rift zones relate to flank instability? Evidence from a collapsing rift at Etna," *Geophys. Res. Lett.*, vol. 39, 2012, Art. no. L20311, doi: 10.1029/2012GL053683
[90] G. Iovine, M. Parise M. and C. Tansi, "Influence of structural setting in the development of the gravity-related phenomena. A study case in Northern Calabria (Italy)," *Supplementi di Geografia Fisica e Dinamica Quaternaria*, vol. 20, no. 1, pp. 93–99, 1997.

Ivana Zinno received the Laurea degree (summa cum laude) in telecommunication engineering and the PhD degree in electronic and telecommunication engineering both from the University of Naples Federico II, Naples, in 2008 and 2011, respectively. In 2011 she received a grant from the University of Naples to be spent at the Department of Electronic and Telecommunication Engineering for research in the field of remote sensing. Since January 2012, she has been with the IREA-CNR (National Research Council), Naples, where she currently holds a researcher position. In 2017 she has been visiting scientist with the Jet Propulsion Laboratory (JPL), Pasadena (CA). Her work is currently focused on the development of advanced Differential SAR Interferometry (DInSAR) techniques for surface deformation time series generation and on the exploitation of distributed computing architectures (GRID and Cloud Computing platforms) for Big SAR Data processing. Her main research interests are in the field of microwave remote sensing; in particular they concern differential SAR interferometry applications, with particular emphasis on novel generation satellite constellations such as Sentinel-1, and, more generally, the information retrieval from SAR data by also exploiting fractal models.

Manuela Bonano received the Laurea degree (summa cum laude) in environmental engineering from the University of Cagliari, Italy, in 2004 and the PhD degree in infrastructures and transportation from the University of Roma "La Sapienza", Italy, in 2012. In 2007 she started her research activity in the SAR interferometry field at IREA-CNR, where her interests were mainly focused on the development of advanced multi-pass interferometry algorithms for full resolution DInSAR analyses of local deformation affecting single buildings and man-made structures. Since 2017 she has been with the Istituto di Metodologie per l'Analisi Ambientale (IMAA-CNR) where she holds a permanent researcher position. In 2011 she was a Visiting Scientist with the Earth and Planetary Science (EPS) Department of University of California at Berkeley (UCB), USA. Currently, she works on the development of advanced DInSAR techniques for processing SAR data acquired by novel generation satellites, such as COSMO-SkyMed, TerraSAR-X, and Sentinel-1, based on the exploitation of advanced distributed computing technologies (HPC and GPU) and infrastructures (GRID and Cloud Computing).

Sabatino Buonanno graduated in computer engineering from the University of Sannio, Italy, in 2003. In 2004 he joined the Mediterranean Agency for Remote Sensing and Environmental Control (MARSec) in Benevento, Italy, where he occupies the position of the person in charge for the systems network of receiving station for satellite data. He took part in different national and international projects such as the "EMSA framework for a satellite monitoring service for Marine oil spill detection and surveillance of European waters" in collaboration with telespazio, several projects for the environmental monitoring using satellite data for the Campania Region. He participated in the coordination of the activities for the certification of MARSec as network station of Canadian Radarsat-1 and Israeli Eros-a satellites. Tenured professor in computer science, he holds the title of PhD at the University "La Sapienza" in Rome, in 2017, with secondments to IREA-CNR. Currently he is outside contractor with IREA, and he is working on SBAS code efficiency, SBAS results management, visualization and integration with other sources of information, in an OGC compliant environment.

Francesco Casu received the Laurea degree (*summa cum laude*) and the PhD degree in electronic engineering from the University of Cagliari, Cagliari, Italy, in 2003 and 2009, respectively. Since 2003, he has been with the IREA-CNR (Italy) where he currently holds a permanent researcher position. He was a visiting scientist with the University of Texas at Austin (2004), the Jet Propulsion Laboratory, Pasadena (2005), and the Department of Geophysics at Stanford University (2009). His main research interests are in the DInSAR field, in the multi-pass interferometry (particularly concerning the improvement of the SBAS-DInSAR algorithm) and in the SBAS-DInSAR measurement assessment, with particular emphasis on novel generation satellite constellations such as COSMO-SkyMed, TerraSAR-X and Sentinel-1. More recently, he has been involved in the development of DInSAR algorithms for unsupervised processing of huge SAR data archives by exploiting High Performance Computing platforms, such as GRID and Cloud computing ones. He is the scientific responsible of the IREA-CNR activities as Center of Competence of the Italian Civil Protection Department. Finally, he acts as a reviewer of several peer-reviewed international journals and he has served as a scientific committee member of a number of international conferences.

Claudio De Luca received the Laurea degree (110/110) in telecommunication engineering from the University of Naples "Federico II", Naples, in 2012 and the PhD degree in computer and automatic engineering from the Department of Electrical Engineering and Information Technology of the University of Naples "Federico II", in 2016. Since January 2013 he has been with IREA (Istituto per il Rilevamento Elettromagnetico dell'Ambiente)—CNR (National Research Council), Naples, where he currently holds a researcher position. His main research interests include the development of advanced Differential SAR Interferometry (DInSAR) techniques for deformation time series generation by also exploiting parallel computing platforms. Recently he has been involved in the field of cloud computing solution for intensive processing of remote sensing data, development of advanced algorithm for Sentinel-1 SAR data processing.

Michele Manunta received the Laurea degree in electronic engineering, in 2001 and the PhD degree in informatics and electronic engineering, in 2009 from the University of Cagliari, Italy, with a thesis on Differential SAR Interferometry. From 2002 he has been with Istituto per il Rilevamento Elettromagnetico dell'Ambiente (IREA), an Institute of the Italian National Research Council (CNR), where he currently holds a researcher position. He was a visiting scientific with the Institut Cartografic de Catalunya (Spain), in 2004, and the Rosenstiel School of Marine and Atmospheric Science of the University of Miami, in 2006. His research interests are in the field of high resolution SAR and DInSAR data processing and application. He particularly works on developing SAR/DInSAR algorithms and techniques for studying deformation affecting terrain surface (such as those produced by landslides, subsidence, volcano activity, and earthquakes) and man-made structures. More recently his research interests concern Cloud and GRID computing exploitation for SAR interferometry applications. He has been collaborating in various national and international initiatives for the exploitation of satellite technologies, and in particular of SAR techniques.

Mariarosaria Manzo received the Laurea degree (summa cum laude) in mathematics from the University of Naples Federico II, Naples, Italy, and the PhD degree in methods and technologies for environmental monitoring from the University of Basilicata, Potenza, Italy, in 1998 and 2008, respectively. In 2002, she joined the Istituto per il Rilevamento Elettromagnetico dell'Ambiente (IREA), Italian National Research Council (CNR), where she currently holds a permanent researcher position. She was a visiting researcher with German Aerospace Center (DLR), Oberpfaffenhofen, Germany, in 2004, and with the Geodesy Laboratory, University of Miami, Coral Gables, FL, USA, in 2007. She has been and is currently involved in several national and international research projects. Her research interests include differential SAR interferometry (DInSAR), particularly, the development of algorithms for the generation of velocity maps and corresponding time series starting from SAR data acquired by the first- and second-generation satellite sensors, and the application of such algorithms for the monitoring of surface displacements, such as those produced by subsidence, volcano activity, earthquakes and landslides. Her current research interests also include the development of optimization/inversion algorithms for the analytical modeling of seismic and volcanic sources by using DInSAR and geodetic data.

Riccardo Lanari (M'91-SM'01-F'13) received the Laurea degree in electronic engineering (*summa cum laude*) from the University of Napoli, Federico II, Napoli, in 1989. In 1989, he joined IRECE and after that IREA, both Research Institutes of the Italian Council of Research (CNR). He has more than 25 years of research experience in the earth observation field, particularly on space-borne synthetic aperture radar (SAR) and SAR interferometry (InSAR) data processing methods developments, and their applications in the geosciences. On these topics, he is the holder of two patents and he has coauthored the book *Synthetic Aperture Radar Processing* (CRC Press, 1999) and 115 peer-reviewed publications on ISI journals that have, nowadays, more than 9500 citations (H-index = 46, source: Google Scholar). He has been a visiting scientist in different foreign research institutes, including the German Aerospace Research Establishment (DLR), Germany (1991 and 1994), the Institute of Space and Astronautical Science (ISAS), Japan (1993), and the Jet Propulsion Laboratory (JPL), CA, USA (1997, 2004, and 2008). He has been adjunct professor of electrical communication with the University of Sannio, Benevento from 2000 to 2003 and, from 2000 to 2008, main lecturer in the Institute of Geomatics in Barcelona, Spain. Moreover, he has achieved the national scientific habilitation as a full professor of telecommunications (December 2013) and as a full professor of geophysics (February 2014). He is (since 2001) a distinguished speaker of the Geoscience and Remote Sensing Society of the IEEE and he has lectured in several national and foreign universities and research centers and served as a chairman/convener and/or Scientific Program Committee member at many international conferences. He is member (from 2015) of the Advisory Board of the Italian Space Agency (ASI) for the COSMO-SkyMed missions of first and second generation and (from 2017) of the National Commission for the Prevision and Prevention of Big Risks (*Commissione Nazionale Grandi Rischi*). He received from NASA a recognition (1999) and a group award (2001) for his activities related to the SRTM project based on the InSAR experiments carried out in 2000, within a mission of the Space Shuttle Endeavour. He received the Dorso prize (2015), for the Special Section "Research," an association for resource development in Southern Italy held under the patronage of the Senate of the Italian Republic. Moreover, he has received the Christiaan Huygens Medal (2017), one of the prizes that the European Geosciences Union awards each year to eminent scientists for their innovations, discoveries, or relevant contributions that have led to significant progress in the area of "Geosciences Instrumentation and Data Systems". Since November 2011, he has been the Director of the IREA-CNR. He is a fellow of the IEEE.